Journal of Nuclear Materials 382 (2008) 190–196

Contents lists available at ScienceDirect

Journal of Nuclear Materials

journal homepage: www.elsevier.com/locate/jnucmat

Cluster-dynamics modelling of defects in α-iron under cascade damage conditions

E. Meslin [a,*], A. Barbu [a], L. Boulanger [a], B. Radiguet [b], P. Pareige [b], K. Arakawa [c], C.C. Fu [a]

[a] Service de Recherches de Métallurgie Physique, CEA/Saclay, 91191 Gif-sur-Yvette cedex, France
[b] Groupe de Physique des Matériaux UMR-CNRS 6634, Equipe de Recherche Technologique, No. 1000, Université de Rouen, B.P. 12, 76801 Saint Etienne du Rouvray, France
[c] Research Center for Ultra-High Voltage Electron Microscopy, Osaka University, 7-1, Mihogaoka, Ibaraki, Osaka 567-0047, Japan

ARTICLE INFO

PACS:
61.82.Bg
61.72.Ff
61.72.Ji

ABSTRACT

We report the calibration of a rate theory numerical code capable to reproduce the agglomeration of point-defects produced in α-iron by irradiation under cascade damage conditions. The input parameters are obtained by performing transmission electron microscopy (TEM) experiments in α-iron. It was irradiated at temperatures between 200 and 400 °C with high flux krypton ion under resolvable point-defect cluster conditions. The TEM analyse of the sample irradiated at the highest temperature reveals the presence of two dislocation loop populations: large ones are decorated with small ones, both vacancy and interstitial in type. The vacancy loops are proposal to be located in the compressive side of the large interstitial loops.

1. Introduction

The neutron irradiation of reactor pressure vessel (RPV) steels causes the increase of the ductile–brittle transition temperature. This mechanical properties degradation is partly due to the formation of nanometer-size solute and point-defect (PD) clusters. Therefore, it is a crucial issue to understand their formation. In high copper content RPV steels, it is generally admitted that a homogeneous precipitation mechanism is at the origin of the experimentally observed copper-enriched clusters [1,2]. However, it has been recently shown that this mechanism cannot explain the formation of such clusters in low copper content FeCu model alloys [3,4]. This conclusion was obtained by irradiating a FeCu-0.1 wt% binary alloy with energetic electrons and ions. The geometry of the samples and the damage rate were chosen to give approximately the same supersaturation of isolated point-defects in both conditions. At variance with ion irradiation, no copper cluster was detected by 3D atom probe (3DAP) after electron irradiation, where only isolated Frenkel pairs are created. The main difference between both kinds of irradiation is the formation of small PD clusters in the core of displacement cascades under ion irradiation, as predicted by results of molecular dynamics (MD) simulations in α-iron [5]. We therefore suggested that the formation of copper rich clusters under cascade damage conditions occurs via a heterogeneous precipitation on PD clusters. Calculations carried out with a rate theory (RT) code, taking simultaneously into account the clustering of point-defects and the formation of copper precipitates, assuming a homogeneous precipitation mechanism [6], confirmed this assumption. Indeed, no significant copper precipitation under cascade conditions was obtained. The PD clusters were modelized by using a code calibrated on transmission electron microscopy (TEM) analyse of ferritic alloys irradiated with 1 MeV electron at high damage rates [7]. This calibration was the beginning of a complete study devoted to the modelling of the irradiation induced damage in α-iron. The first part treated the simple case of electron irradiation and assumed the PD clusters to be immobile, independent of their size. To go further, a more extensive study is carried out within the PERFECT European project [8]. Ferritic model alloys were irradiated with neutrons in the BR2 Belgium test reactor and the resulting damage was characterized by complementary experimental techniques such as 3DAP or TEM. PD clusters larger than about 2 nm are visible by TEM as dislocation loop or cavity, but since the clusters formed under neutron irradiation are small, an important part of the size distribution cannot be given by experiments. They can only be investigated by modelling. For this reason, we undertook the experimental calibration of our rate theory model under cascade conditions by using simple ion irradiated α-iron. To ensure the validity of the calibration, it must be carried out within a large temperature range and account for the mobility of small PD clusters, predicted by previous MD simulations [9] and recent *ab initio* calculations [10,11]. The purpose of this paper is precisely to report the experimental study of the PD clusters induced and to describe the calibration of the rate theory model under cascade damage irradiation.

* Corresponding author. Tel.: +33 1 69082168; fax: +33 1 69086667.
E-mail address: estelle.meslin@cea.fr (E. Meslin).

0022-3115/$ - see front matter © 2008 Elsevier B.V. All rights reserved.
doi:10.1016/j.jnucmat.2008.08.010

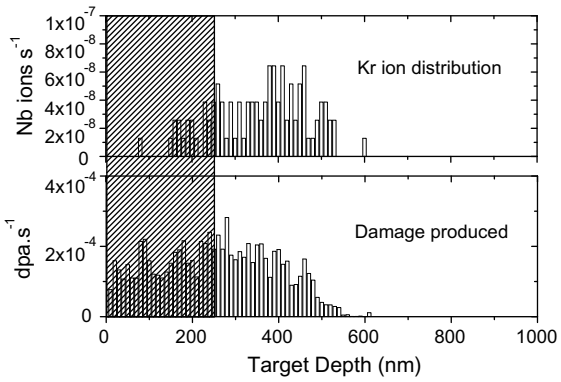

Fig. 1. Damage induced by 1.5 MeV Kr ions in an iron target (SRIM calculation [13]). An energy threshold of 40 eV for the iron atom displacement was chosen. The number of implanted ions per second and the dose rate at each thickness were calculated using an ion flux of 1.1×10^{11} ions cm^{-2} s^{-1}. The dashed area in the figure corresponds to the range of thicknesses visible by TEM, where the damage is likely homogeneous.

2. Experimental study

2.1. Experimental set-up

This study was performed on a pure iron sample provided by the Ecole des Mines of Saint-Etienne. It contains less than 5 wt ppm of carbon and nitrogen and less than 10 wt ppm of silicon. Other elements are less than 1 wt ppm. For TEM investigations, 3 mm disc samples were jet electropolished with a Struers Tenupol 2 device using a solution of 10% perchloric acid and 20% butoxyethanol-2 in ethanol at −40 °C until perforation. With this preparation method, we cannot avoid a slight surface oxidation, which introduces a granite-like contrast on the thin foil. The minimal resolvable size of PD clusters was thus 2 nm. The TEM thin foils were then irradiated in the Van de Graaff accelerator ARTHUR of SRMP/CEA at three temperatures (200, 300 and 400 °C) with 1.5 MeV Kr ions. At this energy, the mean projected range of ions is about 350 nm. Since the relevant thickness of the area observable by TEM is around 100 nm, very few atoms were implanted. Most of them passed through the samples and the damage produced is quite homogeneous in the thin foil (Fig. 1). To be consistent with the previous calibration of the model [7], carried out using 1 MeV electron irradiation, the ion flux was chosen to obtain the same damage rate: 1.5×10^{-4} dpaNRT s^{-1}. It was calculated within the simplified NRT approach [12] with the SRIM code [13]. We obtained an ion flux equal to 1.1×10^{11} ions cm^{-2} s^{-1}. We checked that under these conditions, the sputtering rate is very low, equal to 1.7×10^{-7} ion s^{-1}. The irradiation doses were optimized to obtain a damage quantitatively analysable by TEM. The alloys were thus irradiated at 200 °C up to 1.2 dpaNRT, 300 °C up to 0.48 dpaNRT and 400 °C up to 0.2 and 0.5 dpaNRT.

After irradiation, classical TEM observations were performed in a Philips CM20 electron microscope to determine the number density, the size distribution and the nature of dislocation loops. To avoid a possible effect of grain orientation due to the surface image force acting on the loops [14], the number densities were always calculated in {100} orientated grains. These densities were obtained by plotting the projected number density Δp as a function of sample thickness. For this purpose, two images under different diffracting conditions were performed (Fig. 2). The first one is in two-beams dynamical conditions to measure the thickness using similar thickness fringes and the second one is in kinematical conditions to obtain a better contrast of dislocation loops. The number density of dislocation loops is $\Delta L = \Delta p/(e - 2 \cdot Z_d)$, where e and Z_d are the thicknesses of the thin foil and of the denuded zone near the surface, respectively.

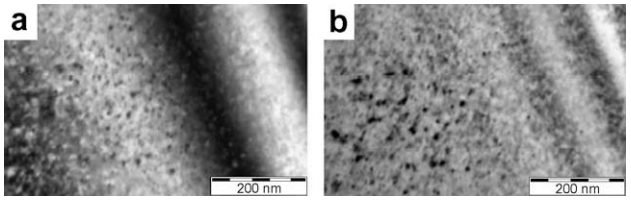

Fig. 2. Determination of the loop number density. The thickness of the specimen at each point is first obtained by using similar thickness fringes (a) in dynamical conditions and the number of loops in each area is calculated (b) in kinematical conditions. See text for more details.

Several techniques can be used to determine the nature of dislocation loops, depending on their size [15]. The loops with a diameter larger than 10 nm were investigated by the classical method of external/internal contrast [16]. For the smaller ones, as the direct methods of black/white analysis or 2 1/2D technique, based on stereomicroscopy, are difficult to apply and have been shown to be inefficient, e.g. in copper [17], we used an indirect determination based on the bias dependence of dislocation loops, already used in α-iron [18]. The bias factor of dislocation loops for self-interstitial atoms (SIA) is larger than for vacancies (V), independent of the loop nature. This difference leads to a net flux of SIA toward loops of both nature. Then, interstitial loops grow whereas vacancy ones shrink during electron irradiation. This is the reason why we performed 2-MeV electron irradiation on the Kr ion irradiated sample in the HVEM Hitachi 3000 of the University of Osaka.

2.2. Results

TEM observations show that when the temperature increases from 200 to 400 °C, the trends of loops number density is to decrease when their size increases (Table 1 and Fig. 3). Also, the width of the distribution increases with temperature (black distribution in the Fig. 4).

After irradiation at 400 °C and 0.5 dpaNRT, the loops are large enough so their Burgers vector and nature can be easily analysed. Fig. 5 shows that two loop populations are present: one is located randomly in the thin foil and has a mean diameter of 20 nm and the other is in the vicinity of the first one, with a smaller mean diameter of 8 nm. We noticed that the most appropriate imaging conditions to see the two loop populations are obtained when the grains are orientated close to a ⟨110⟩ zone axis, as for the Fig. 5 and the Fig. 6(e). The former has a poor quality because it was obtained while the specimen was tilted over a large angle. We can yet distinguish small loops. The Burgers vector analyse of the larger loops revealed that most of them are ⟨100⟩ loops (Fig. 6), but a few 1/2⟨111⟩ ones were also observed. This atypical character of iron compared with other bcc metals, where the dislo-

Table 1
Number density (ΔL) and mean diameter ($\bar{d}$) of loops formed in the studied material irradiated at different temperatures

T	Dose		ΔL	$\bar{d}$
(°C)	(ions cm^{-2})	(dpaNRT)	(cm^{-3})	(nm)
200	8.7 10^{14}	1.2	>10^{16}	10 ±4
300	3.5 10^{14}	0.48	3 ±1 10^{15}	15 ±7
400	1.4 10^{14}	0.20	2 ±0.5 10^{15}	18 ±9

Doses in ions cm^{-2} were calculated by measuring the ion beam current each 7 min using Faraday cages. Doses in dpaNRT were obtained with the SRIM code [13]. The indicated error bar on the mean loop diameter $\bar{d}$ is the statistical standard deviation.

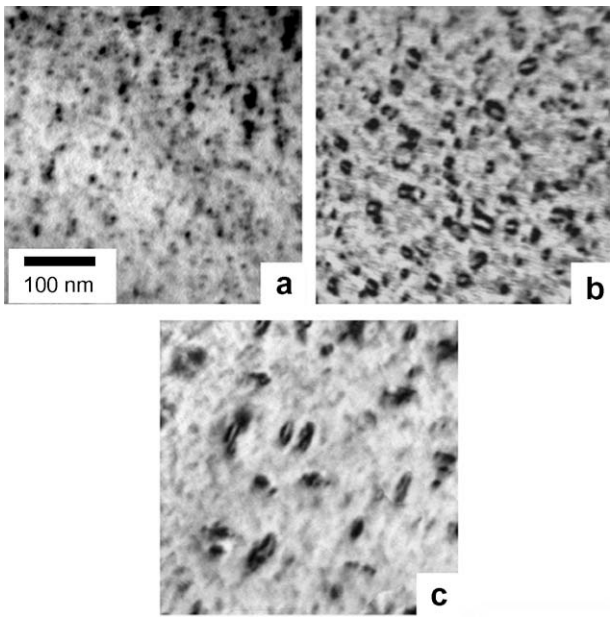

Fig. 3. BFTEM images of the ion irradiated alloys at three temperatures (a) 200 °C, (b) 300 °C and (c) 400 °C.

cation loops are mainly $1/2\langle 1\,1\,1\rangle$, is in agreement with many previous results [19–23]. To go further, we tried to obtain the nature of these two populations. The first one is large enough to allow the use of the classical internal/external contrast method [16], which was applied to the circled dislocation loops in Fig. 6. First, their Burgers vector **b** was defined using

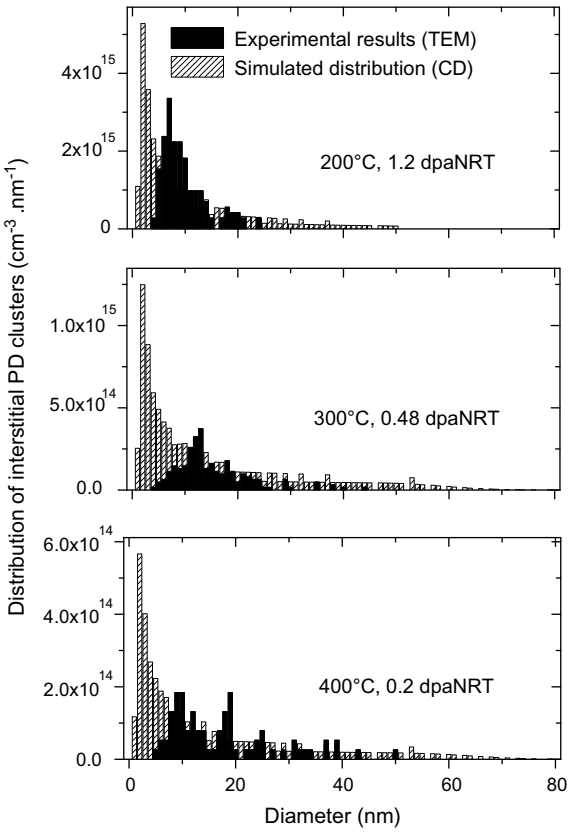

Fig. 4. Comparison between the distribution of visible loops determinated by TEM and calculated with the calibrated model.

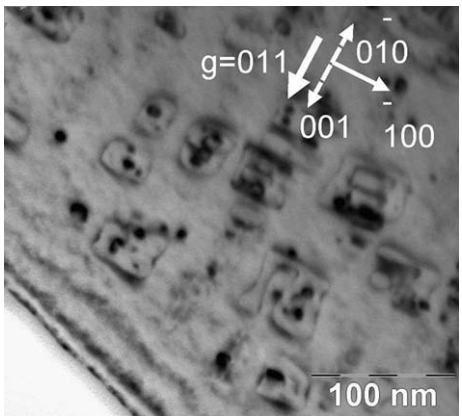

Fig. 5. Dislocation loops formed after irradiation at 400 °C up to 0.5 dpaNRT. Two loop populations are clearly visible. The diffracting condition is $\mathbf{g} = \langle 0\,1\,1\rangle$ and $z = [0\,\bar{1}\,1]$ (BFTEM).

the FS/RH (perfect crystal) convention. The dislocation line sense is defined to be clockwise around the loop. According to the standard diffraction contrast technique [16], since the loops are visible with the diffraction vector $\mathbf{g} = \langle 1\,1\,0\rangle$ (Fig. 6(b)) and invisible with $\mathbf{g} = \langle 0\,2\,0\rangle$ and $\mathbf{g} = \langle 0\,\bar{1}\,1\rangle$ (Fig. 6(d) and (e)), their Burgers vector can only be $a\langle 1\,0\,0\rangle$. The next step was to evaluate the sense of **b**. In the Fig. 6(a), the loops are close to the edge-on configuration. Consequently, they are almost prismatic. Furthermore, they present an external contrast in the Fig. 6(b), which means that the triple scalar product $\mathbf{g}\cdot\mathbf{b}\cdot\mathbf{s}$ – where **s** is the deviation parameter – is positive. Thus, **b** has the same sense as **g**, which is also the sense of the upwards normal of the loops ($\mathbf{n_{100}}$), indicated in the image in dash line. As a consequence, large loops are interstitial in nature. The same interpretation can be performed from Fig. 6(c), where the loops are in internal contrast. To determine the nature of the smaller loops, the sample was irradiated with 2 MeV electrons at 400 °C. We focused on the behavior of the loop 1 in Fig. 7. Before the electron irradiation ($t = 0$ s), it is located on the vicinity of the large interstitial loop 2. Then, the loop 2 grows ($t = 23.6$ s) and disappears ($t = 24$ s), probably absorbed by the nearest loop 3 or eliminated on the surface. At the time $t = 30$ s, the loop 1 begins to shrink until it vanishes ($t = 36$ s). Loop 1 is therefore vacancy in type. It should be noted that small growing interstitial loops were also seen. The localization of some vacancy loops (V-loops) next to the large interstitial loops (I-loops) may result from the trapping of V-loops in the compressive strain field of the dislocation. It should be noticed that these mechanism is not limited to cascade damage conditions since it was observed in nickel after electron irradiation also [24]. As it was already pointed out by Urban [24], as long as the V-loops are located in the compressive strain field of the interstitial loop, they are stable because the I-loops absorb the freely migrating SIA from the surroundings. But when the V-loops are not in the strain field any more, less vacancies than interstitials are eliminated on them and they shrink.

3. Model calibration

3.1. Cluster-dynamics model

3.1.1. Model description

Cluster-dynamics modelling is a mean field approach which allows the study of the long term evolution of point-defect clusters [7]. The clustering of mobile species, isolated or forming clusters, is described within the assumption that there are no spatial correlations between species. Particular interactions are replaced by

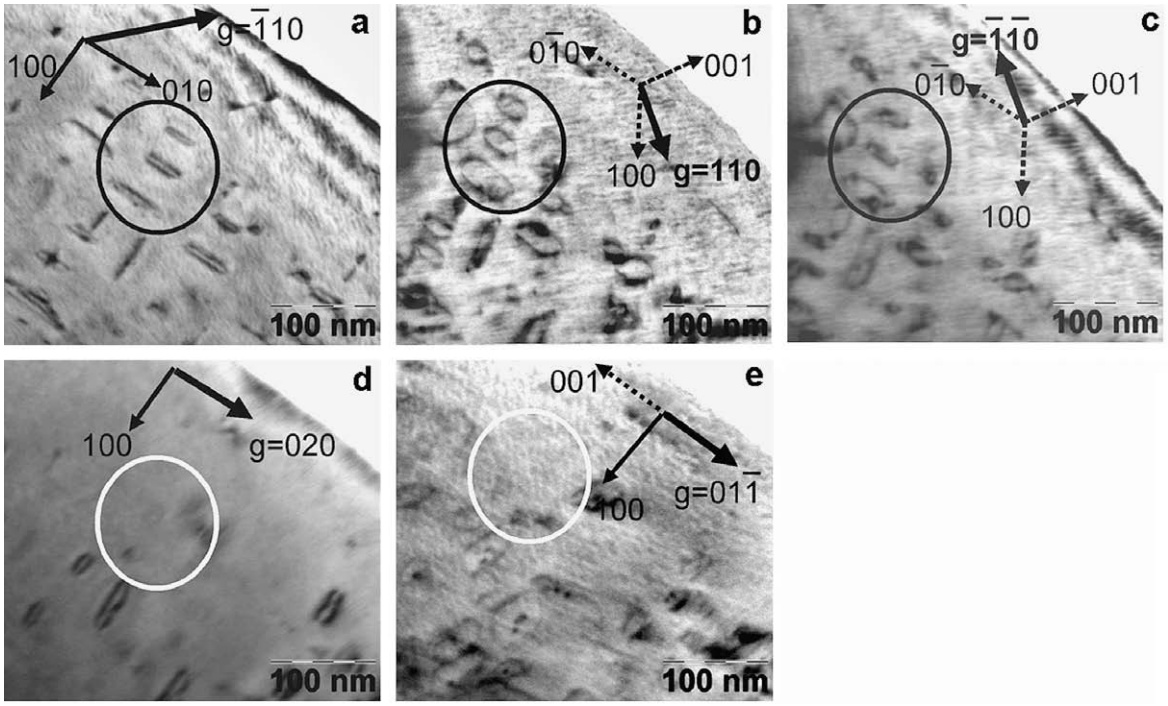

Fig. 6. Determination of the Burgers vector and nature of the large loops formed under ion irradiation up to 0.5 dpaNRT at 400 °C. BFTEM images of the same area imaged with $s > 0$ under the following diffracting conditions: (a) $\mathbf{g} = \langle \bar{1}\,1\,0 \rangle$, $z = [0\,0\,1]$; (b) $\mathbf{g} = \langle 1\,1\,0 \rangle$, $z = [1\,\bar{1}\,1]$; (c) $\mathbf{g} = \langle \bar{1}\,\bar{1}\,0 \rangle$, $z = [1\,\bar{1}\,1]$; (d) $\mathbf{g} = \langle 0\,2\,0 \rangle$, $z = [0\,0\,1]$ and (e) $\mathbf{g} = \langle 0\,1\,\bar{1} \rangle$, $z = [0\,1\,1]$. Solid lines refer to directions in the plan on the foil whereas dash lines refer to projected upwards directions.

average ones. This assumption permits to follow the evolution of cluster size distribution over time corresponding to RPV steels lifetime within short computation time. The evolution of the number density C_j of clusters containing j point-defects is controlled by the balance equation

$$\frac{dC_j}{dt} = G_j + \sum_k w(k,j)C_k - \sum_k w(j,k)C_j - L_j, \quad (1)$$

where $w(k,j)$ and $w(j,k)$ are the creation and the elimination rate of a j-size cluster by absorption or emission of a k-size cluster, G_j the production rate of clusters of size j and L_j the elimination rate of clusters on fixed sinks such as dislocations, grain boundaries or surfaces. Notice that G_j stands for the source term to take into account the isolated point-defects and PD clusters remaining in the displacement cascades after their relaxation stage.

3.1.2. Parameters

To use this model, we need to know the input parameters. Some of them are intrinsic to the material, such as the sample thickness or the grain size, and others are energetic and kinetics parameters, like the formation or migration energies of species, controlling the rate of capture and emission of point-defects by clusters. In the previous model calibration [7], it was assumed that only monomers were mobile and the energetics parameters were adjusted on experiments. It was recently modified to introduce the mobility of PD clusters and their creation in displacement cascades. As the predictive power of models is linked to the validity of the parameters used, in this study, the energetic parameters were not adjusted but resulted from *ab initio* calculations performed recently in α-iron [10,11,25]. The parameters used are reported in Table 2.

3.2. Experimental calibration

3.2.1. Calibration after ion irradiation

The calibration was performed on the size distribution and on the number density of interstitial loops obtained after ion irradiation at 400 °C and 0.2 dpaNRT. As we aimed to reproduce the irradiation damage of a TEM thin foil, it is assumed that the sink strength of grain boundaries is negligible in comparison with that of surfaces.

The parameters relative to pure iron, free of carbon, were used. However, in the present case, carbon implantation may occur during the irradiation in the ion accelerator, as it was previously observed on tomographic atom probe needles [26]. It must be taken into account since previous *ab initio* calculations suggest an attractive interaction of vacancies with impurities: carbon or nitrogen atoms [27]. As a result, in the range of temperatures studied, vacancies may be mainly trapped by carbon atoms to form complexes. If we assume that these complexes are not mobile, the effective mobility of V in iron-containing-carbon is lower than in pure one. The reason is that the dissociation of complexes is needed to allow the long range diffusion of V. It should be noted that such a trapping was experimentally observed after HVEM experiments of α-iron of different purities [28]. To take into account the presence of carbon, the effective diffusion coefficient of vacancies was adjusted on TEM experiments. By assuming a pre-exponential factor equal to 8.2×10^{-3} cm^2 s^{-1}, we found an effective migration energy of 0.83 eV. There is a good agreement with a recent experimental adjustment of the desorption rate in α-iron using a rate theory model as well [29]. They found the same value of 0.83 ± 0.08 eV.

Moreover, to describe the source term, a set of new parameters (f_n^θ) was introduced. Each of them is defined by $f_n^\theta = G_n^\theta \cdot nV/G$, where θ can be either an interstitial or a vacancy, G_n^θ is the number density of clusters containing n point-defects θ, V, the iron atomic volume and G, the defect production rate. The latter is equal to $\eta \cdot G_{NRT}$. G_{NRT} is the damage rate calculated within the NRT approach [12] and η is the fraction of PD clusters remaining after the mutual SIA–V recombination calculated by MD [30] with respect to the NRT approach.

In a first step, we performed the calculation assuming that only isolated Frenkel pairs were created by irradiation. The source term

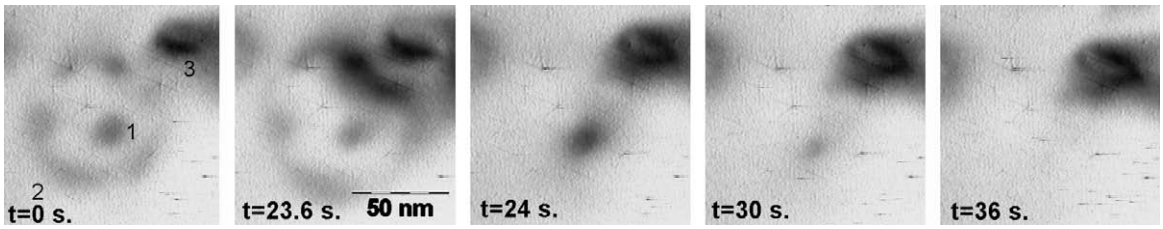

Fig. 7. Evolution of dislocation loops during 2 MeV-electron irradiation at 400 °C. The irradiation times are given (BFTEM). See text for more details. Black impacts visible on the figures correspond to the damage generated by the CCD camera degradation under electron irradiation.

was only composed of two terms, f_1^I and f_1^V, both equal to one. The resultant PD clusters number density was equal to 1.2×10^9 cm^{-3}, several orders of magnitude lower than the experimental value of $2 \pm 0.5 \times 10^{15}$ cm^{-3} (Table 1). Then, we used a source term provided by MD cascade simulation (Fig. 8). In that case, the calculated number density, equal to 9.07×10^{17} cm^{-3} was overestimated. It is not surprising for two reasons: (i) the cluster-dynamics model, as every model based on rate theory, is not well adapted to describe the strongly correlated objects such as displacement cascades and (ii) molecular dynamic simulations treat only the first stages of cascade relaxation. Many point-defects may be eliminated during their annealing. Finally, an effective source term distribution was used to reproduce experimental results. As we consider the I- and V-clusters to be mobile up to a size of 3 and 4, respectively (Table 2), we chose a simplified source term including only some I_4 and V_5, the first immobile clusters. The result is given in Table 3. It is worth noticing that only a small proportion of immobile point-defect clusters is needed in the source term to constitute the stable nucleus of PD clusters. Since the results are very sensitive to temperature, we checked the model prediction at two different temperatures: 200 °C and 300 °C. The agreement with the experiment was found to be reasonable (Fig. 4). Notice that a large proportion of small PD clusters obtained by modelling were not clearly visible by TEM, certainly because of the slight oxide layer on the surface of the samples.

3.2.2. Calibration after neutron irradiation

We used the TEM results of a study performed within the PERFECT European project [31] on the same material as for the previous calibration. Contrary to ion irradiation, the neutron irradiation was realized on the bulk material. In this case, the sink strength of surfaces is negligible compared with the sink strength of grain boundaries. The samples were irradiated at a flux of 9.5×10^{13} $n_{E>1\text{MeV}}$ cm^{-2} s^{-1}, corresponding to a damage rate of 1.3×10^{-7} dpaNRT s^{-1} and doses from 0.025 to 0.2 dpaNRT at 300 °C. The adjustment was performed on the interstitial dislocation loops distribution given in the Fig. 9. The fitted empirical source term is reported in Table 3. It should be noticed that 80% of vacancies form clusters. Furthermore, by comparison with the source term obtained to reproduce Kr ion irradiation, when the incident particles are neutrons, the proportion of point-defects in clusters is higher than that of ion irradiation. The cascades are 'harder', which means that the mean energy of primary knocked on atom (PKA) is shift toward higher energies, as shown in the Fig. 10.

To check our calibration, we used an experimental study by Eldrup et al. [32]. Iron specimens, containing 50 wt ppm of impurities, were irradiated at 70 °C with neutron at increasing doses from 1×10^{-4} to 0.72 dpaNRT and at a dose rate of 6×10^{-7} dpaNRT s^{-1}. PD clusters formed during irradiation were characterized by Positron Annihilation Spectroscopy (PAS) and TEM. Open volume such as vacancy clusters can be detected by PAS experiments. The V- and I-cluster number densities calculated using our calibrated model were compared with the PAS and TEM results. The results plotted in Fig. 11 show that, even at 70 °C, the CD calculations are in relative good agreement with experimental results, considering

Table 2
Parameters used for the cluster-dynamics modelling of the pure iron

Parameter	Value
Pre exponential factor: D_{0i}; D_{0v}	8.2×10^{-3} cm^2/s
E^m: I, I_2, I_3, $I_{n>3}$	0.34, 0.42, 0.43 eV, ∞
E^m: V, V_2, V_3, V_4, $V_{n>4}$	0.67, 0.62, 0.35, 0.48 eV, ∞
E^f: I, V	3.64, 2.2 eV
E^B, I–I, I_2–I, I_3–I	0.83, 0.92, 1.64 eV
E^B: V–V, V_2–V, V_3–V, V_4–V	0.3, 0.37, 0.62, 0.73 eV
Z_I^d, Z_V^d	1.1, 1
TEM thickness foil	120 nm
Grain size	200 μm
Recombination radius	0.65 nm
Dislocation density	10^8 cm^{-2}
D_{min} (loop or cavity)	2 nm
η	0.3

Energetic parameters can be found in Refs. [10,11,25]. E^m, E^f and E^B refer respectively to migration, formation and binding energies. The binding energies of clusters $I_{n>3}$–I and $V_{n>4}$–V were obtained by using a capillary law given in the Ref. [7]. D_{0x} is equal to $a_{bcc\ Fe}^2 \cdot \nu$, where $a_{bcc\ Fe}$ is the *bcc* iron lattice parameter and ν, the frequency of lattice vibration (10^{13} Hz). Z_θ^d is the capture efficiency of point-defects θ by dislocations, D_{min} refers to the minimal diameter of defects visible by TEM and η is the fraction of point-defect remaining after the mutual SIA–V recombination. We used a value calculated by molecular dynamics [30].

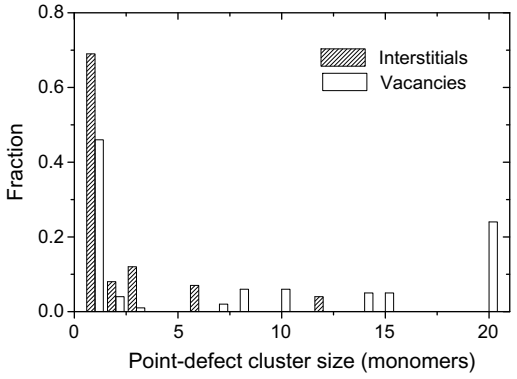

Fig. 8. Distribution of point-defects, isolated and forming clusters, used to simulate a real cascade. The details of the calculation is given in Appendix.

Table 3
Simplified source term and effective migration energy of vacancies used to reproduce krypton ion and neutron irradiation

Source term	Kr ion	$f_4^I = 1.10^{-4}, f_5^V = 0.05$
	Neutron	$f_4^I = 3.10^{-4}, f_8^V = 0.8$
E_{eff}^m (V)	Kr ion and neutron	0.83 eV

The others f^I and f^V terms are equal to zero, except the fraction of monomers θ, either interstitial or vacancy in type, deduced from: $f_1^\theta = 1 - \sum_{n>1} f_n^\theta$.

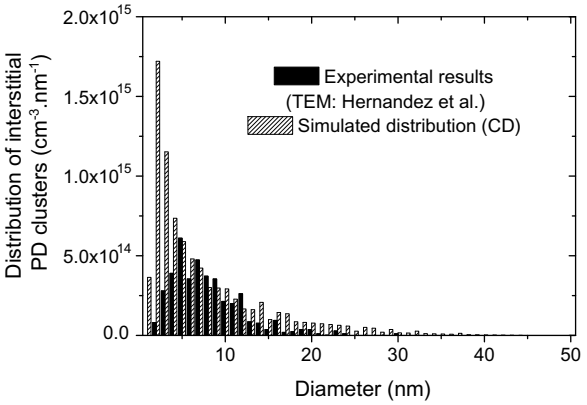

Fig. 9. Adjustment of the RT model on TEM results obtained by Hernandez et al. on an α-iron neutron irradiated up to 0.2 dpaNRT [31].

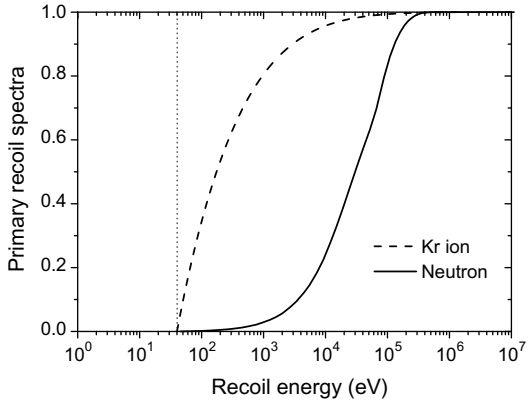

Fig. 10. Normalized primary recoil spectra generated by 1.5 MeV Kr ions and by the neutron spectrum considered in this study. They were calculated with the DART software [35].

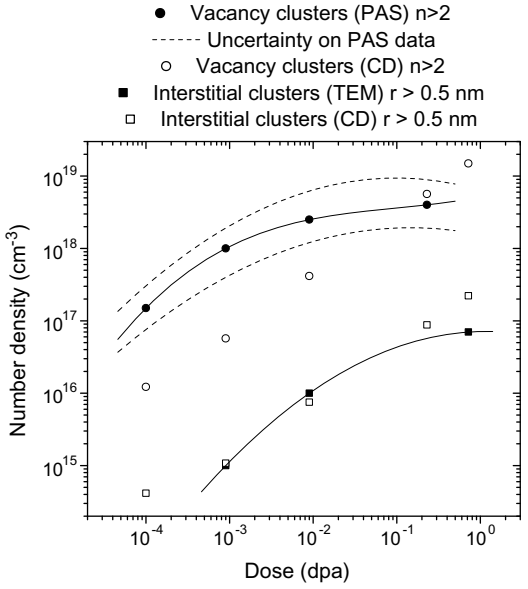

Fig. 11. Comparison between the interstitial and vacancy clusters number densities calculated with our calibrated model and the experimental results obtained by Eldrup by PAS and TEM [32].

the experimental uncertainties and approximations made in the model. It constitutes a validation of our calibration.

4. Conclusions

The main goal of this paper was to give the optimized parameters of a numerical rate theory code under cascade irradiation conditions. For this purpose, krypton ion irradiation of an iron-containing-carbon – a carbon implantation certainly occurred during the irradiation – was performed from 200 to 400 °C. The TEM study of the sample irradiated at 400 °C reveals that two loop populations are present. Indeed, large interstitial loops are decorated with small ones, both interstitial and vacancy in type. As it was already suggested [24], vacancy loops may be located in the compressive strain field of large interstitial loops. Furthermore, the quantitative analyse of the visible interstitial clusters was used to calibrate the source term of the code after krypton ion irradiation. The energetics parameters resulted from *ab initio* calculations performed in α-iron [10,11,25]. In particular, the mobility of small point-defect clusters was taken into account. However, the migration energy of single vacancies was increased up to 0.83 eV, to consider their mobility slowing-down in presence of carbon atoms [27]. The calibration of the source term after neutron irradiation was performed using experimental results obtained at 300 °C on the same material [31] irradiated in the BR2 test reactor. As a consequence, the parameterized model is able to reproduce the damage induced by krypton ion and neutron in an iron-containing-carbon. The next step is to calibrate the model to reproduce the point-defect clusters formed in binary FeCu alloys, e.g. assuming that the copper effect is only to increase the binding energy of di-interstitials [7]. The comparison between the calculated PD clusters number density and the experimental TAP copper clusters number density will provide us information about copper clusters formation mechanism in low copper FeCu alloys. That will be the topic of a future publication.

Acknowledgements

The authors thank Dr Y. Serruys from CEA/SRMP for the ion irradiations and acknowledge the support of the PERFECT European Integrated Project under Contract No. FI6O-CT-2003-508840.

Appendix. MD based calculation of the source term of the cluster-dynamics model

The point-defects clusters formed in displacement cascade are considered in our RT code within the source term *G*. The produc-

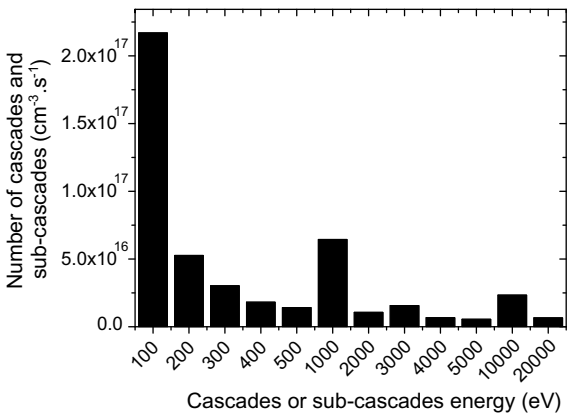

Fig. 12. Cascade and sub-cascade spectra generated by the irradiation of an iron target. See text for the details of the calculation.

tion rate G_n^θ of n-size PD clusters has the expression: $G_n^\theta = (G/V_{at}) \cdot (f_n^\theta/n)$, where the normalized coefficient f_n^θ is the proportion of PD included in n-size PD clusters with respect to the total number of PD in PD clusters.

The distribution of point-defects clusters remnant after the cooling stage of displacement cascades was calculated by combining three approaches: the Lindhart formalism [33], the SRIM software [13] and the Molecular Dynamics. The latter can provide the PD clusters generated by PKA of energy lower than 20 or 40 keV. We used cascades of energy lower than 20 keV calculated in the pure iron at 600 K [34]. For higher energies, sub-cascades are formed so the PKA can be replaced by the sub-cascades they generated. Primary spectra resulting from our irradiation conditions (1.5 MeV Kr ion) was calculated within the Lindhart formalism. The proportion of PKA with an energy higher than 20 keV has the following expression:

$$p_\sigma^{T>20\text{ keV}} = \frac{\int_{20\text{ keV}}^{T_{max}} \sigma(T)dT}{\int_{E_d}^{T_{max}} \sigma(T)\mathrm{d}T}, \quad (2)$$

where $\sigma(T)$ is the differential energy cross section, T the PKA energy, E_d the energy threshold for the iron atom displacement and T_{max} the maximum energy transferred by an 1.5 MeV Kr ion to an iron atom. $p_{v\sigma}^{T>20\text{ keV}}$ is limited to 1.5%. Nevertheless, the proportion of damage generated by these energetics PKA with respect to the total damage is high. It is expressed by

$$p_{v\sigma}^{T>20\text{ keV}} = \frac{\int_{20\text{ keV}}^{T_{max}} \nu(T)\sigma(T)\mathrm{d}T}{\int_{E_d}^{T_{max}} \nu(T)\sigma(T)\mathrm{d}T}. \quad (3)$$

$\nu(T)$ is the number of PD generated by a PKA with an energy T. It was calculated within the classical NRT approach [12]. We obtained a proportion of 69.7%. To take account of these PKA, we used the TRIM software [13]. The PKA of energy greater than 20 keV were replaced by the sub-cascade they generated. The distribution in energy of cascades and sub-cascades obtained is given in the Fig. 12. The convolution of this distribution with the population of PD clusters calculated by MD provided us the source term of our RT model. It was previously given in the Fig. 3.

References

[1] C. Liu, G. Odette, B. Wirth, G. Lucas, Mater. Sci. Eng. A 238 (1997) 202.
[2] M.H. Mathon, A. Barbu, F. Dunstetter, F. Maury, N. Lorenzelli, C. de Novion, J. Nucl. Mater. 245 (1997) 224.
[3] B. Radiguet, A. Barbu, P. Pareige, J. Nucl. Mater. 360 (2007) 104.
[4] P. Pareige, B. Radiguet, A. Barbu, J. Nucl. Mater. 352 (2006) 75.
[5] A. Calder, D. Bacon, J. Nucl. Mater. 207 (1993) 25.
[6] F. Christien, A. Barbu, J. Nucl. Mater. 324 (2004) 90.
[7] A. Hardouin-Duparc, C. Moingeon, N.S. de Grande, A. Barbu, J. Nucl. Mater. 302 (2002) 143.
[8] <www.fp6perfect.net>.
[9] R.E. Stoller, J. Nucl. Mater. 233–273 (1996) 999.
[10] C.C. Fu, F. Willaime, P. Ordejón, Phys. Rev. Lett. 92 (2004) 175503.
[11] F. Willaime, C.C. Fu, M.C. Marinica, J.D. Torre, Nucl. Instrum. and Meth. B 228 (2005) 92.
[12] M.J. Norgett, M.T. Robinson, I.M. Torrens, Nucl. Eng. Des. 33 (1975) 50.
[13] J.F. Ziegler, Nucl. Instrum. and Meth. B 219&220 (2004) 1027.
[14] W. Jäger, M. Rühle, M. Wilkens, Phys. Status Solidi (a) 31 (1975) 525.
[15] M.L. Jenkins, J. Nucl. Mater. 216 (1994) 124.
[16] P.B. Hirsch, A. Howie, R.B. Nicholson, D.W. Pashley, M.J. Whelan, Electron Microscopy of Thin Crystals, Robert E. Krieger, New York, 1969.
[17] H. Kukushima, M. Jenkins, M. Kirk, Philos. Mag. 75 (1997) 1567.
[18] M. Horiki, T. Yoshiie, M. Iseki, M. Kiritani, J. Nucl. Mater. 271&272 (1999) 256.
[19] N. Yoshida, M. Kiritani, F.E. Fujita, J. Phys. Soc. Jpn. 39 (1) (1975) 170.
[20] A.E. Ward, S.B. Fisher, J. Nucl. Mater. 166 (1989) 227.
[21] A.C. Nicol, M.L. Jenkins, M.A. Kirk, Mater. Res. Soc. Proc. 650 (2001) R1.3.1.
[22] D.T. Hoelzer, F. Ebrahimi, Mater. Res. Soc. Proc. 373 (1995) 57.
[23] B.C. Master, Philos. Mag. 11 (1965) 881.
[24] K. Urban, Phys. Status Solidi (a) 4 (1971) 761.
[25] C.C. Fu, J.D. Torre, F. Willaime, J.-L. Bocquet, A. Barbu, Nat. Mater. 4 (2005) 68.
[26] B. Radiguet, PhD thesis, Rouen University, 2004.
[27] C. Domain, C.S. Becquart, J. Foct, Phys. Rev. B 69 (14) (2004) 144112.
[28] A. Hardouin-Duparc, PhD thesis, Paris XI-Orsay University, 1998.
[29] C.J. Ortiz, M.J. Caturla, C.C. Fu, F. Willaime, Phys. Rev. B 75 (10) (2007) 100102.
[30] D.J. Bacon, A.F. Calder, F. Gao, J. Nucl. Mater. 251 (1997) 1.
[31] M.H. Mayoral, D.G. Briceño, PERFECT Project, Advance Report, Deliverable P26, Task II-3-2.
[32] M. Eldrup, B.N. Singh, S.J. Zinkle, T.S. Byun, K. Farrell, J. Nucl. Mater. 307–311 (2002) 912.
[33] J. Lindhart, V. Nielsen, M. Scharff, Mat. Fys. Medd. Dan. Vid. Selsk. 36 (1968) 1.
[34] C. Domain, J. Ruste, C.S. Becquart, Etude par simulation numTrique du dommage d'irradiation, Application au fer pur et aux alliages fecu, Tech. Rep., 1998.
[35] L. Lunéville, D. Simeone, C. Jouanne, J. Nucl. Mater. 353 (2006) 89.